https://doi.org/10.5194/nhess-2022-173
Preprint. Discussion started: 20 July 2022

Natural Hazards and Earth System Sciences
Discussions

Sensitivity analysis of a built environment exposed to debris flow impacts with 3-D numerical simulations

Xun Huang[1,2], Zhijian Zhang[1], Guoping Xiang[3,4]

[1]Geography and Tourism College, Chongqing Normal University, Chongqing, 401331, China
[2]Chongqing Key Laboratory of Surface Process and Environment Remote Sensing in the Three Gorges Reservoir Area, Chongqing Normal University, Chongqing, 401331, China
[3]405 Geological Brigade of Sichuan Bureau of Geology & Mineral Resources, Dujiangyan, 611830, China
[4]State Key Laboratory of Geohazard Prevention and Geoenvironment Protection, Chengdu University of Technology, Chengdu, 610059, China

Correspondence to: Xun Huang (huangxun@cqnu.edu.cn)

Abstract. The characteristics of exposed built environments have a significant effect on debris flow impacts on buildings, but knowledge about their interactions is still limited. This paper presents a sensitivity analysis on the overall peak impact forces on a building resulting from the built environment parameters, including the orientation, opening scale of the target building, and azimuthal angle and distance of surrounding buildings. The impact forces were obtained using the FLOW-3D model, a computational fluid dynamics approach, verified through the physical modeling results. The results show that the surrounding buildings' properties have significant roles in determining the peak impact forces. A shielding effect or canalization effect, which reduce or increase impact forces, respectively, can be produced by changing the azimuth angle. A deflection wall for building protection is recommended according to the shielding effect. A narrowed flow path, determined by both the azimuth angle and distance, has a significant effect on the variation in impact forces. In addition, it is concluded that a splitting wedge should be designed following a criterion of avoiding the highest flow velocity - the smallest approaching angle - appearing near the longest wall element. The protruding parts caused by changing the building's orientation contribute to increasing impact loads within a shielding area. A limited opening effect is observed on the whole building if there is sufficient time for material intrusion. The insights gained contribute to a better understanding of building vulnerability indicators and local migration design against debris flow hazard.

1 Introduction

In mountain environments, buildings are the elements of greatest concern with regard to debris flow hazard risks (Zeng et al., 2015; Fuchs et al., 2019; Luo et al., 2020). Compared to strong structures such as railway bridges, common residential buildings are more easily damaged by debris flows (Hu et al., 2012; Huang and Tang, 2014). Furthermore, the damage to buildings has been demonstrated to contribute greatly to casualties and property loss based on a large number of catastrophic debris flow events (Tang et al., 2011; Zhang et al., 2018; Chen et al., 2021). In recent decades, the understanding, assessment and eventual reduction in building exposure and vulnerability have been brought into focus in mountain hazard mitigation (Holub and Fuchs, 2009; Fuchs et al., 2015, 2017).

In the classical S-shaped vulnerability curves, a quantitative assessment approach based on interactions between process intensities and building damage, considerable ranges in the loss ratio were found for moderate process intensities (Fuchs et al., 2012). This is in good agreement with the fact that two buildings located exactly at the same place, despite experiencing the same process intensity, do not always suffer the same degree of loss (Papathoma-Köhle, 2016; Papathoma-Köhle et al., 2017). Process intensity is not decisive in terms of building damage, and some building characteristics of the building itself and its surroundings play critical roles in the degree of damage induced by debris flow. This understanding has also been confirmed by the spatial distribution of building damage ratios in the debris flow torrents of the Austrian Alps (Fuchs et al., 2012).

Currently, the characteristics of an exposed building, including the orientation, openings and surrounding environments, have been reported to be important to the impact forces of torrential hazards (Jakob et al., 2012; Sturm et al., 2018a). As far as building orientation is concerned, it is commonly recommended to individually analyze wall elements of different orientations. It is widely accepted that walls with faces perpendicular to the stream are generally exposed to higher dynamic pressures due to the larger effective contact area (Mead et al., 2017; Manawasekara et al., 2016). However, limited studies to date have examined the impact performance of a whole building. In terms of building openings such as windows, doors and light shafts, it is well established that the impact forces on the building envelope tend to decrease once the flow penetrates openings (Mazzorana et al., 2014; Gems et al., 2016). However, this process is regarded to be at the expense of greater building loss due to the higher impact forces on interior walls and greater indoor property losses (Totschnig et al., 2011; Mead et al., 2017). Recent developments regarding the surroundings of built environments have attracted much attention. The existence of surrounding buildings definitely reduces the impact forces on a particular building due to the deflection of the flow and the shielding of the element at risk; however, this may also increase the impact forces by redirecting or canalizing the flow and forcing the flow to impact the building (Gao et al., 2017; Sturm et al., 2018b). Therefore, it remains difficult to make a general statement regarding whether the effect of surrounding buildings is negative or positive (Sturm et al., 2018a).

Although considerable efforts have been devoted to the relationships between building characteristics and debris flow impacts, only some simple trends, rather than quantitative results about the effects of factors, have been determined. Knowledge regarding the interactions between the built environment parameters and impact loads is still limited, and considerable research gaps still exist regarding (1) the identification of the built environment parameters with the greatest influence on debris flow impacts; (2) detailed explanations of each built environment factor; and (3) the interrelations between these parameters.

Because field measurement of debris flow impacts is nearly impossible, laboratory experiments and numerical modeling are regarded as feasible alternatives for capturing interactions, and they may provide insights into the impact of debris flows in the interior and against the exterior of buildings (Gems et al., 2016; Papathoma-Köhle, 2016). In this study, a sensitivity analysis was conducted based on 3-D numerical simulation, and the effects of various built environment factors on the impact forces of debris flows were quantitatively analyzed and compared. Debris flow numerical simulations were conducted using the FLOW-3D model, a commercial Computational Fluid Dynamics (CFD) program. Kim et al. (2021) conducted a sensitivity analysis of five parameters for fine sediment trapping and energy reduction with a debris flow slit-type barrier via a FLOW-3D numerical model and metamodels. These kinds of methods offer opportunities for performing a sensitivity analysis with limited data (Kim et al., 2019, Kim et al., 2021). These results can be applied to determine the indicators and to improve weightings for reliable building vulnerability assessment and to enhance the knowledge about built environment improvement and local migration design.

In the following, the reliability of the numerical model was first confirmed by comparison with a physical flume test executed by Song et al. (2021). A sensitivity analysis was then performed using metamodels and global sensitivity analysis (GSA). The built environment parameters considered in this study were the orientation (***Or***) and opening scale (***Op***) of the target building and the azimuthal angle (***A***) and distance (***D)*** of the surrounding buildings. Finally, the effects of each parameter and their interactions on the peak impact forces of the overall building were explained in detail.

2 Numerical modeling of debris flow

2.1 Model description

The identification of complex geometry and three-dimensional flow tracking are the key steps in the process-response simulation between buildings and debris flows. However, the current numerical codes used for debris flow simulations consider the flow depth to be small relative to the tangential length scale and simplify this factor to represent shallow water flow. They have only second-order accuracy in space, as the effects of complex three-dimensional topography and the vertical mobility of debris flows are not considered (Zhang et al., 2021b). To avoid the above-mentioned limitations, it is necessary to use an efficient 3-D numerical approach to accurately capture the debris flow behaviors considering the influences of building geometry.

FLOW-3D, a three-dimensional finite-volume-based CFD model, is considered one of the most efficient tools for predicting hydraulic phenomena with strong turbulent components and inconsistent free water surfaces. FLOW-3D was designed to address the Reynolds-Averaged Navier–Stokes equations (RANS) (Jones and Launder, 1972), implementing the Volume of Fluid (VOF) methods (Hirt and Nichols 1981) and Fractional Area/Volume Obstacle Representation (FAVOR) (Hirt and Sicilian, 1985). The advanced Tru-VOF method can be used to precisely track the three-dimensional transient free fluid surface. Its unique FAVOR mesh processing technology can define independent and complex geometry within the structured mesh and avoid the shortcomings of the traditional finite difference method in complex boundary fitting (Zhang et al., 2021b). As a result of a robust capacity to deal with the data in both the fluid and solid phases, the FLOW-3D code is considered to be appropriate for analyzing the interactions between debris flows and exposed buildings.

https://doi.org/10.5194/nhess-2022-173
Preprint. Discussion started: 20 July 2022

To consider turbulence and viscosity in FLOW-3D, the renormalized group model (RNG)-based K-epsilon turbulence model (k-ε) is utilized, which uses statistical formulations to compute the turbulent kinetic energy dissipation rate (Franco et al., 2021). In recent years, the RNG model has been applied in simulations of landslide surges (Yin et al., 2015; Hu et al., 2020), the entrainment effects of debris avalanches (Hu et al., 2019), dam-break floods (Zhuang et al. 2020), and the runout characteristics of debris flows (Zhang et al., 2021b), with good results. In this study, a series of debris flow simulations based on the RNG model with various building characteristics were executed. Because the overall building damage is considered the focus of building risk assessment in debris flow prone areas (Prieto et al., 2018), the General Moving Objects (GMO) model of FLOW-3D was applied to obtain the overall impact forces on the building, in which a rigid body motion was introduced for the fluid-rigid interaction behavior (Postacchin, 2019; Isobe, 2021). To reduce the uncertainty, the peak impact forces of debris flows were obtained from the average values over 10 points (Song et al., 2021).

2.2 Validation with flume test

A debris flow impact experiment against a rigid obstacle conducted by Song et al. (2021) was adopted to validate the FLOW-3D model due to the dedicated measurement of the total impact pressure on the obstacle. The test ID of 50-100-15 was further selected due to its representative flip-through impact phenomenon. Flip-through impact is commonly observed in an elevated flow front as a hydraulic jump as debris flows surge into flat terrain (Méjean et al., 2020), or secondary waves overtake the flow front (Iverson et al., 2010). In flip-through impact, the measured impact pressure on the obstacle could be on the order of 10-100 times the hydrostatic pressure associated with the impacting wave height (Lugni et al., 2006). Therefore, flip-through impact plays a significant role in determining the debris flow impact load on the elements at risk.

A bilinear flume, with a 15° upstream section and 5° downstream section, was constructed (Fig. 1a). The upstream end of the flume was isolated with a storage container with an uplift gate for debris material release. The height of gate uplift was limited to 100 mm in the validated test group. A rigid plate 800 mm high and 300 mm wide was erected perpendicular to the flume bed 2145 mm downstream of the smooth transition zone. A total of six 12 mm diameter miniature load cells were embedded into the rigid barrier to measure the impact pressure of the debris flow (Fig. 1b). In the 50-100-15 test group, the solid concentration of the debris flow was 50%, the viscosity of the fluid phase was 0.1 Pa·s, and the bulk density was 1878.2 kg/m^3.

In the numerical simulation, the targeted analysis domain was discretized into a grid with a cell size of 0.02 m. In FLOW-3D, a surface roughness parameter (Rr), defined as the equivalent grain roughness (or absolute height in meters), can be set for every solid body included in the model domain (Franco et al., 2021). The simulation time was set to 5.0 s to correlate with the corresponding flume test. The debris flow properties, such as the solid concentration, viscosity and bulk density, were set to be the same as those in the physical experiment. The flow process and peak impact forces were compared to validate the accuracy of the numerical simulation.

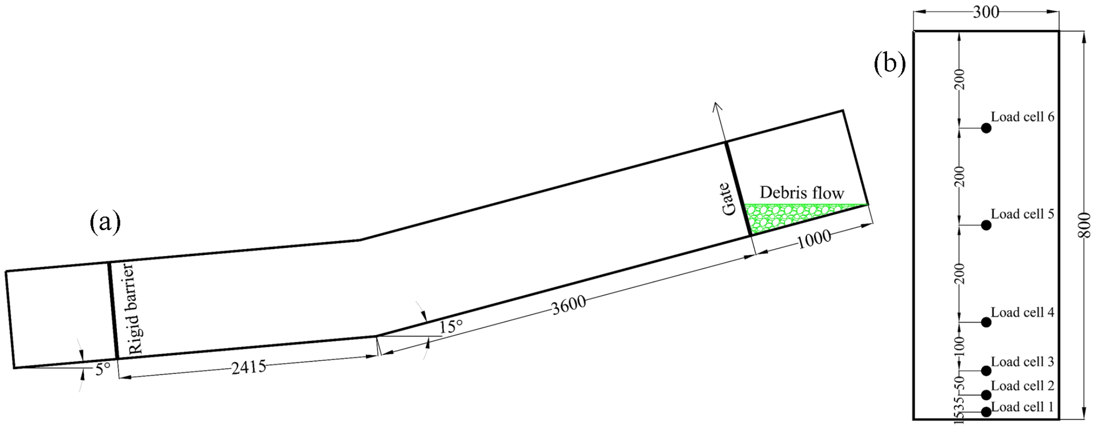

Figure 1. A schematic drawing of the experimental setup and instrumentation in Song et al. (2021): (a) flume setup; (b) rigid barrier for measurement of total impact pressure. All dimensions in mm.

The computed surface profile of the debris flow at approximately 3.0 s after release from the storage container is shown in Fig. 2. As described by Song et al. (2021), there is an obvious flip-through impact in the fall back stage of the simulated debris flow. Specifically, the concave face of the wave first approached the obstacle with the crest moving forward (Fig. 2a and Fig. 2a'), then a trough rose rapidly at the barrier (Fig. 2b and Fig. 2b'), and finally, an accelerated jet was formed (Fig. 2c and Fig. 2c'). It is concluded that using the VOF method in the FLOW-3D model can reflect the key information of the dynamic evolution of debris flow impact on an obstacle. Furthermore, load cells 1, 2 and 3 were selected to investigate the variation in the peak impact forces. Table 1 shows the simulated and measured peak impact forces considering the impulse loads due to flip-through impact. The deviations of the peak impact pressures from the three load cells are only -12%, -3% and 9%, respectively. FLOW-3D reproduces the debris flow impact process in the flume test very well.

Table 1. Comparison of debris flow peak impact forces.

Measuring items	Test	Simulation	Deviation
Load cell 1# (kPa)	8.91	7.84	-12%
Load cell 2# (kPa)	7.66	7.44	-3%
Load cell 3# (kPa)	6.09	6.63	9%

2.3 Numerical model set up

As shown in Fig. 3, a depositional fan model with a length of 120 m, width of 120 m, monogradient of 5°, and surface roughness (Rr) of 0.05 m was numerically constructed. A debris flow inflow with a time-invariance discharge of 500 $m^3 s^{-1}$, an initial velocity of 10 $m s^{-1}$, and a flow duration of 10.0 s was set at the top center of the depositional fan. The inflow profile was rectangular, with a channel base width of 20 m, flow depth of 2.5 m and inclination angle of 5°. The real debris flow was simplified as a viscous fluid with a bulk density of 2000 $kg m^{-3}$ and a viscosity of 1.0 Pa·s, close to the viscous debris flow. The impact load on a whole building was considered to be provided only by the debris flow slurry, therefore, the size effect in granular materials was neglected in this study.

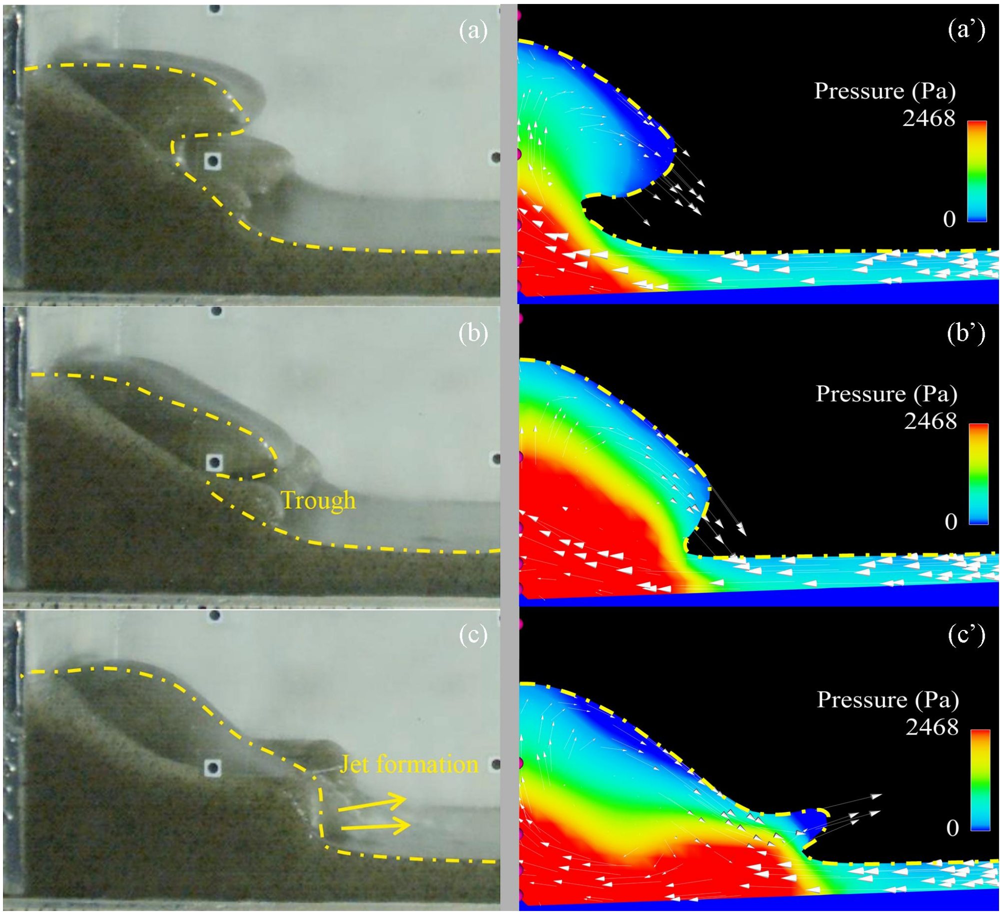

150 **Figure 2. Comparisons between the measured (a-c) (Song et al., 2021) and simulated results (a'-c') on the evolution of a flip-through impact for flume test 50-100-15. (a) and (a') show the concave face of wave approaching the obstacle; (b) and (b') show a trough rapidly rising; (c) and (c') show an accelerated jet formation.**

The focus of this study is the debris flow peak impact forces on the target building, as shown in red in Fig. 3, under the influence of various built environment parameters. The target and surrounding building models, with a length of 15 m, width of 10 m, height of 6 m (equal to 2 floors) and wall thickness of 0.35 m, were designed in accordance with representative buildings in the mountainous areas of southwestern China, including the Wenchuan earthquake areas. To maintain a balance between the computational accuracy and time cost, the cell size of the target-building domain was set to 0.25 m, and the rest of the computational domain was discretized to intervals of 0.5 m. The total number of computational cells was 1,645,600. The planar center of the target building was set 80 m downstream of the debris flow inflow, as shown in Fig. 3.

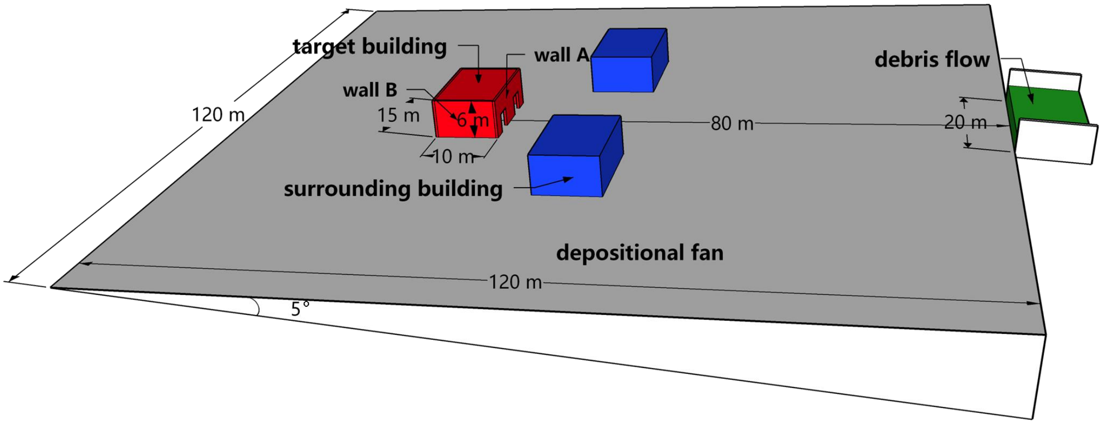

Figure 3. Overview on the components of three-dimensional deposition fan model for debris flow impact simulation on buildings.

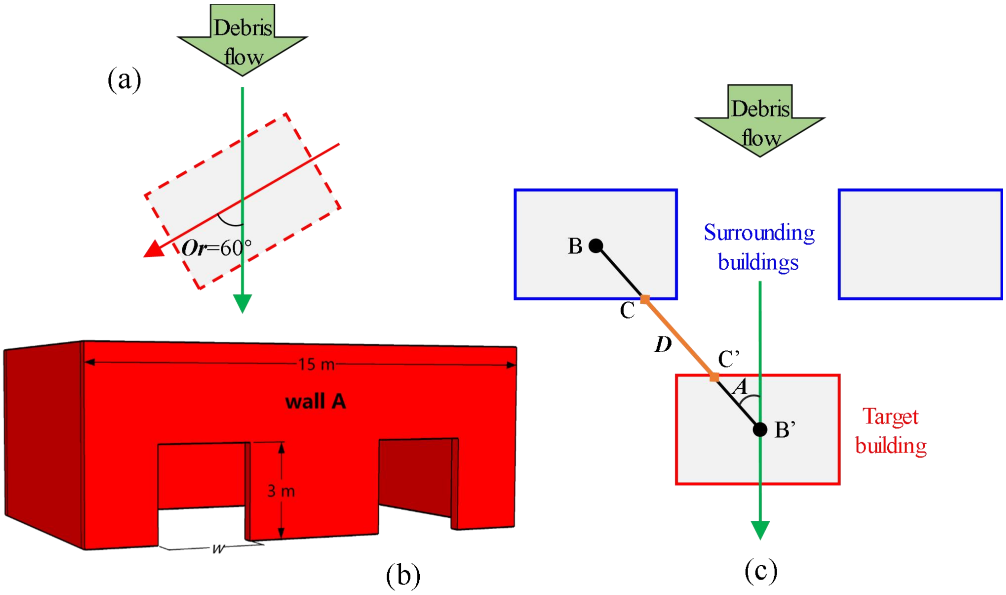

Figure 4. The schematic drawings of the target building and surrounding buildings: (a) orientation of target building (*Or*); (b) opening scale of the target building (*Op*); and (c) azimuth angle (*A*) and distance (*D*) of surrounding building with respect to the target building.

Because sensitivity analysis requires extensive simulation results to consider the combinations of all the factors, the representative factors that could be adjusted in the FLOW-3D simulation were chosen (Kim et al., 2021). The orientation (***Or***) and opening scale (***Op***) of the target building and the azimuthal angle (***A***) and distance (***D***) of the surrounding buildings with respect to the target building were considered to be the key built environment parameters for debris flow impact loads.

In this study, the orientation (***Or***) of the target building was defined as the angle between the building's long axis and the debris flow's main flow path, as shown in red and green in Fig. 4a and ranged from 0° to 90°. An orientation of 0° meant that the long axis of the building was parallel to the debris flow path, and the perpendicular case was represented by an orientation of 90°. As far as building openings are concerned, it is well known that several features of openings are of great importance in terms of building damage, such as which wall they are located on and their size, height and structure (Gems et al., 2016; Faisal et al., 2018; Papathoma-Köhle et al., 2019). However, it remains challenging to analyze these parameters with a model. In this study, the size of the opening was only selected to be analyzed to reduce computing costs. As shown in Fig. 4b, two symmetrical openings with a constant height of 3 m were placed in wall A. Therefore, the opening scale (***Op***) was defined as the proportion of the total opening width (double *w*) to the length of wall A.

The azimuthal angle (***A***) of the surrounding buildings was defined as the angle between the line of the geometric center of buildings (e.g., line B-B' in Fig. 4c) and the main flow path (green line in Fig. 4c). There were no surrounding buildings downstream of the target building. Except for the scenario of azimuthal angle 0°, two surrounding buildings were placed symmetrically on both sides of the target building. The distance (***D***) between the surrounding building and target building was defined as the straight-line distance between two points located on the overlap between the line of the buildings' geometric centers and building envelope, as shown by the orange line C-C' in Fig. 4c.

3 Sensitivity analysis

3.1 Metamodel modeling

Abundant simulation results are required for assessing the effect of built environment parameters on the debris flow impact force. Due to the considerable time consumed and computational cost, a mathematical metamodel was constructed using a small fraction of the simulation results. A metamodel, referred to as a surrogate model, is a 'model of a model', a simplified model of an actual model using mathematical construction. Numerous accurate simulation results can be generated based on the metamodel relation or algorithm between input and output (Booker et al., 1999; Hoffman et al., 2003). Of the various metamodel modeling methods, the Kriging model - or Gaussian process (GP) - is considered to be the most suitable for the unbiased prediction of a deterministic model and is also fitted to simulation I/O data obtained for global experimental areas (Kleijnen, 2016). In this study, the GP was selected and executed through JMP® Pro 16.0.0, a commercial statistical software designed by SAS Institute Inc.

In this study, the metamodels representing the objective function were created using the 160 cases shown in Table 2. The coefficient of determination (R^2) of regression analysis in the GP model was 0.86. At this accuracy, a total of 10,000 new simulation results were obtained from random values in the specified ranges of the four input variables for use in the subsequent sensitivity analysis.

Table 2. Simulation conditions.

Group	Number of cases	Target building's properties		Surrounding buildings' properties	
		Orientation (***Or***, °)	Opening scale (***Op***)	Azimuth angle (***A***, °)	Distance (***D***, m)
A1[a]	5	0, 30, 45, 60, 90	0.4	45	15
A2	25	0	0.4	0, 30, 45, 60, 90	5, 10, 15, 20, 30
A3	25	30	0.4	0, 30, 45, 60, 90	5, 10, 15, 20, 30
A4	25	60	0.4	0, 30, 45, 60, 90	5, 10, 15, 20, 30
A5	5	90	0, 0.2, 0.4, 0.6, 0.8	45	15
A6	25	90	0.2	0, 30, 45, 60, 90	5, 10, 15, 20, 30
A7	25	90	0.4	0, 30, 45, 60, 90	5, 10, 15, 20, 30
A8	25	90	0.6	0, 30, 45, 60, 90	5, 10, 15, 20, 30
B1[b]	5	0, 30, 45, 60, 90	0	null	null
B2	3	45	0.4	0	5, 10, 15
B3	5	90	0, 0.2, 0.4, 0.6, 0.8	null	null

[a] Simulations group 'A' were designed for the metamodel modeling.
[b] Simulations group 'B' were designed for the detailed interpretations of sensitivity analysis results.

3.2 Sensitivity analysis

Sensitivity analysis aims to understand the relative importance of uncertain input variables to the model response (Zhang et al., 2021a). As opposed to local sensitivity analysis, GSA can be performed by an all-at-a-time method, where output variations are induced by varying all input factors simultaneously, and thus, the sensitivity of each factor considers the direct influence of the factor as well as the joint influence caused by the factor interactions (Kim et al., 2019). GSA allows a ranking among the input parameters to be established according to their influence on the variability of the output. In this study, GSA was conducted to simultaneously consider both the main and interaction effects of input parameters on debris flow impact. A variance-based GSA (VBSA), also referred to as Sobol's indices, is usually recommended. This method is applicable over the whole space of random input data and can also deal with nonlinear responses and measure the effect of interactions in nonadditive systems (Saltelli et al., 2010). The basic principle of Sobol's indices is that the variance of model output is decomposed into fractions within a probabilistic framework that can be attributed to inputs and sets of inputs (Sobol, 1993):

$$\mathrm{V} = \mathrm{Var}[\mathrm{f}(\mathrm{x})] = \sum_{\mathrm{i}=1}^{\mathrm{d}} \mathrm{V}_{\mathrm{i}} + \sum_{1\le \mathrm{i}<\mathrm{j}\le \mathrm{d}}^{\mathrm{d}} \mathrm{V}_{\mathrm{ij}} + \dots + \mathrm{V}_{1,2,\dots,\mathrm{d}} \qquad (1)$$

where the partial variances are calculated as follows:

$$\mathrm{V}_{\mathrm{i}_1,\dots,\mathrm{i}_\mathrm{s}} = \int \mathrm{f}^2_{\mathrm{i}_1,\dots,\mathrm{i}_\mathrm{s}}\left(\mathrm{x}_{\mathrm{i}_1},\dots,\mathrm{x}_{\mathrm{i}_\mathrm{s}}\right)\mathrm{p}\left(\mathrm{x}_{\mathrm{i}_1},\dots,\mathrm{x}_{\mathrm{i}_\mathrm{s}}\right)\mathrm{dx}_{\mathrm{i}_1},\dots,\mathrm{x}_{\mathrm{i}_\mathrm{s}},\ \mathrm{s}=1,\dots,\mathrm{d} \qquad (2)$$

Sobol's indices are defined as the relative contribution of the partial variances to the total variance following the decomposition in Eq. (1)

$$\mathrm{S}_{\mathrm{i}_1,\dots,\mathrm{i}_\mathrm{s}} = \frac{\mathrm{V}_{\mathrm{i}_1,\dots,\mathrm{i}_\mathrm{s}}}{\mathrm{V}} = \frac{\mathrm{V}_{\mathrm{i}_1,\dots,\mathrm{i}_\mathrm{s}}}{\sum_{\mathrm{i}=1}^{\mathrm{d}} \mathrm{V}_{\mathrm{i}} + \sum_{1\le \mathrm{i}<\mathrm{j}\le \mathrm{d}}^{\mathrm{d}} \mathrm{V}_{\mathrm{ij}} + \dots + \mathrm{V}_{1,2,\dots,\mathrm{d}}} \qquad (3)$$

such that:

$$\sum_{i=1}^{d} S_i + \sum_{1 \le i < j \le d} S_{ij} + \dots + S_{1,2,\dots,d} = 1 \quad (4)$$

where the index S_i measures the separate contribution of each variable x_i to the output variance without interaction with any other inputs; hence, S_i is commonly referred to as the first-order effect index or the main effect index. The higher-order indices in Eq. (4) measure the interactive contribution to the total variance. Using S_i, S_{ij} and higher-order indices, we can therefore infer the impacts of each input variable and the interaction of variables on the output variance (Zhang et al., 2021a). In this study, only the second-order effect index, reflecting the interaction between every two factors, was considered. The total contribution of variable i is as follows:

$$S_i^T = \sum_{\{i\} \subset \{i_1,\dots,i_s\}} \frac{V_{i_1,\dots,i_s}}{V} \quad (5)$$

which measures the contributions of variable x_i and its interactions to the output variance. If the input x_i has a S_i^T=0.5, then it contributes 50% of the overall variance of output. In Sobol sensitivity analysis, the input factors with a sensitivity index below 0.01 are usually considered noninfluential to the output (Sarrazin et al., 2016). Unlike the first-order indices,

$$\sum_{i=1}^{d} S_i^T \ge 1 \quad (6)$$

because the interaction effect between, for example, x_i and x_j is included in both S_i^T and S_j^T. The sum of S_i^T is equal to 1 if and only if the model is purely additive without any interaction effects.

In this study, Sobol's global sensitivity indices were calculated using the SobolGSA model, a general purpose GUI-driven GSA software developed by Kucherenko and Zaccheus (https://www.imperial.ac.uk/process-systems-engineering/research/free-software/sobolgsa-software/). SobolGSA evaluates the effect of a factor while all other factors are varied as well, and thus, it accounts for interactions between variables and does not depend on the choice of a nominal point like local sensitivity analysis methods. The set of available GSA techniques includes screening method- (the Morris measure), variance- (Sobol' indices, FAST) and derivative-based sensitivity measures. All techniques implemented in SobolGSA make use of either quasi-Monte Carlo sampling based on Sobol sequences or standard Monte Carlo sampling (Sobol et al., 2011; Kucherenko et al., 2015).

4 Results and discussion

4.1 Results of global sensitivity analysis

Global sensitivity indices and total sensitivity indices for debris flow impacts are listed in Table 3, and the main and total effects of each parameter are expressed in Fig. 5. From the main effect indices, the peak impact force is most sensitive to the azimuth angle, with a maximum value of 0.5144, which represents 51.44% of the overall variance in the debris flow peak impact loads. The most influential second-order effect index, with a value of 0.1861, was obtained for the interaction between the azimuth angle and the distance of the surrounding buildings. This result also highlights the importance of the surrounding buildings' azimuth angle to the debris flow impact over the distance's main effect index of 0.0213. The sums of

https://doi.org/10.5194/nhess-2022-173
Preprint. Discussion started: 20 July 2022

all main effect and second-order effect indices are 0.7072 and 0.2928, respectively, indicating that single built environment parameters have a more significant effect on the debris flow impact on a building.

From the total effect indices, on the other hand, the importance of the built environment parameters to the debris flow impact responses are ranked as follows: azimuth angle (***A***) > orientation (***O*r**) > distance (***D***) > opening scale (***Op***), and their total effect indices are 0.7894, 0.2606, 0.2173 and 0.0255, respectively. The sum of the main effects of the target building's properties (***Or*** + ***Op***) is 0.152, and that of the surrounding buildings' properties (***A*** + ***D***) is 0.531, indicating that the surrounding buildings' properties are more significant than the target building's properties on the peak impact forces.

Finally, it is concluded that the azimuth angle and distance of the surrounding buildings and the target building's orientation are the key factors and must be carefully considered in the assessment of building vulnerability to debris flow impacts. It is highly recommended to further study the effect of the surrounding buildings' azimuth angles. Furthermore, although the scale of building openings indeed has a nonsignificant effect on debris flow impacts in this study, the other features of building openings, such as their location, height and structure, should be discussed in more depth.

Table 3. Global sensitivity indices and total sensitivity indices.

Input variables	***Or***	***Op***	***A***	***D***
Or	0.1647	0.0079	0.0797	0.0083
Op	0.0079	0.0068	0.0092	0.0016
A	0.0797	0.0092	**0.5144**	**0.1861**
D	0.0083	0.0016	0.1861	0.0213
Total effects	0.2606	0.0255	0.7894	0.2173

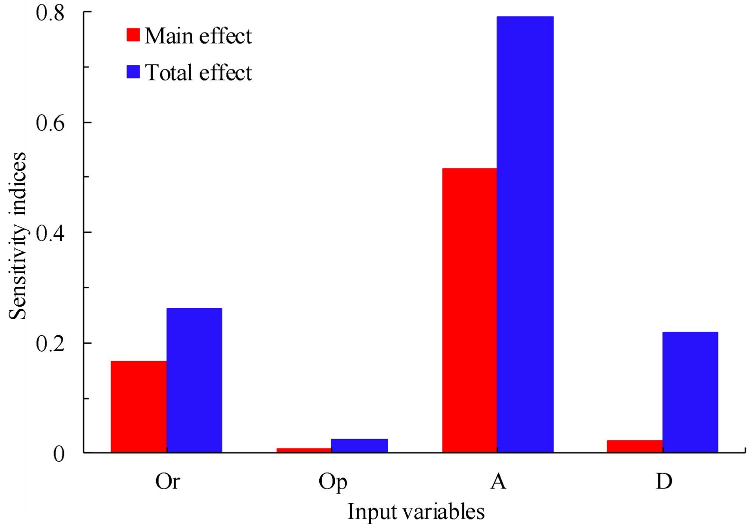

Figure 5. Main and total effects of parameters for debris flow peak impact forces.

4.2 Effect of the surrounding buildings' azimuthal angles

As shown in Fig. 6, the peak impact forces of the debris flow change with increasing azimuth angle in the simulation scenarios at an orientation of 90°, an opening scale of 0.4 and a distance of 5 m (***Or***90-***Op***0.4-***A***x-***D***5, where x represents a variable). The variations in the peak impact forces are calculated with the background value of 3694 kN from the scenario with an orientation of 90°, opening scale of 0.4 and no surrounding buildings (***Or***90-***Op***0.4-***A***null-***D***null, where null means the value is not relevant). The azimuth angles have different kinds of effects on debris flow impacts, as shown in the different colored zones in Fig. 6:

(1) Shielding effect: In the cases of azimuth angles of 0° (***Or***90-***Op***0.4-***A***0-***D***5) and 30° (***Or***90-***Op***0.4-***A***30-***D***5), the peak impact forces are only 1156 kN and 1352 kN, and the corresponding variations (ΔF) are -68.71% and -63.40%, respectively, which are located in the blue region (ΔF < -10%) in Fig. 6. It is indicated that the target building is protected effectively in a shielding area produced by the surrounding buildings. This result is consistent with previous case studies wherein some representative catastrophic debris flow events were observed. In the Zhouqu debris flow event shown in Fig. 7, which occurred in Gansu Province of northwestern China, on 7 August 2010, building B, next to the extensively damaged building A, suffered no damage apart from its first story being buried (Hu et al., 2012). Similarly, in the Qipan gully debris flow case (Zeng et al., 2015), which occurred in Wenchuan city of southwestern China during rainstorms on 11 July 2013, building B, shielding protected from the completely damaged building A, was exposed to only slight damage, as shown in region I of Fig. 8. As shown in Fig. 9, a deflection wall was designed following the principles of the shielding effect and can be repeatedly used to protect an entire building ensemble from gravitational mass movements, such as the snow avalanches, in the mountain areas of Austria (Holub et al., 2012). This design of local protection can provide an effective reference for debris flow mitigation.

(2) Canalization effect: As reported by Sturm et al. (2018a) through flume tests, the existence of surrounding buildings may narrow the flow path and even redirect debris flows, leading to an increasing process intensity toward other buildings (Gao et al., 2017). In these numerical simulations, the azimuth angle of 45° (***Or***90-***Op***0.4-***A***45-***D***5) has the most significant canalization effect on the target building and produces the steepest rise in the peak impact force, with 48.40% growth to a maximum value of 5482 kN, as shown in the orange region (ΔF > 10%) of Fig. 6. As shown in region IV of Fig. 8, building I was exposed to extensive damage in the Qipan gully debris flow partly because of the canalization effect induced by surrounding building J.

(3) Noneffect: The peak impact forces in cases of azimuth angles of 60° (***Or***90-***Op***0.4-***A***60-***D***5) and 90° (***Or***90-***Op***0.4-***A***90-***D***5) are 3662 kN and 3676 kN, respectively, close to the background value (3694 kN), and the corresponding variations are also close to 0, located in the green region (-10% ≤ ΔF ≤ 10%) of Fig. 6. This indicates that there are very small or even negligible effects on the impact loads of the target building. It is important to highlight that the shielding effect has the greatest influence on debris flow impact loads because this effect yields the maximum variation in peak impact forces.

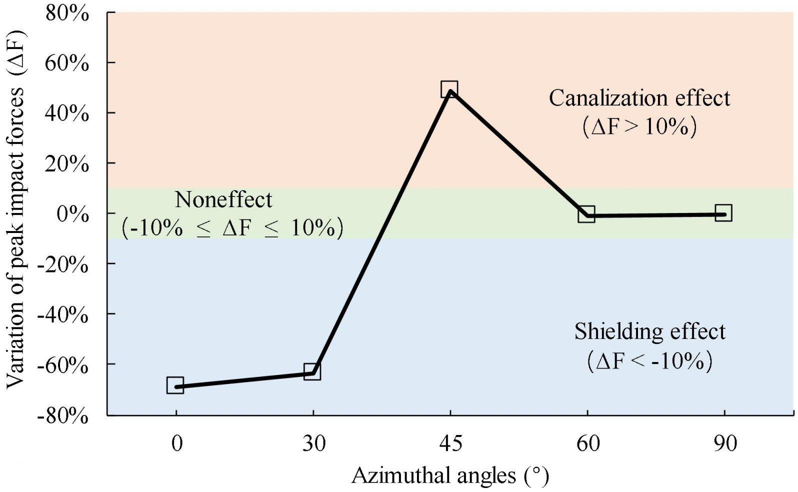

Figure 6. Variations of peak impact forces with increasing azimuth angles in scenarios of orientation 90°, opening scale 0.4 and distance 5 m (*Or*90-*Op*0.4-*A*x-*D*5).

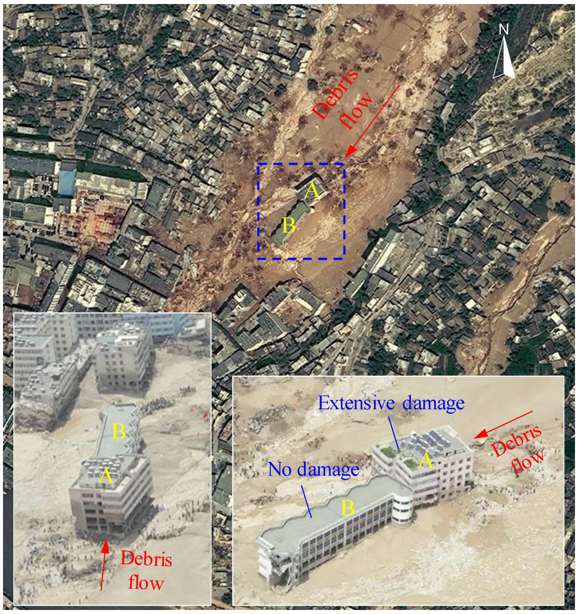

310 **Figure 7. Distribution of damaged-buildings in Zhouqu debris flow event. Orthophoto map is from Digital Globe's WorldView-2 satellite on 22 October 2010 published by NASA (ref: https://earthobservatory.nasa.gov/images/45329/landslide-in-zhouqu-china); Aerial photo is referred from website of http://slide.news.sina.com.cn/c/slide_1_5039_12703.html (Tang et al., 2011).**

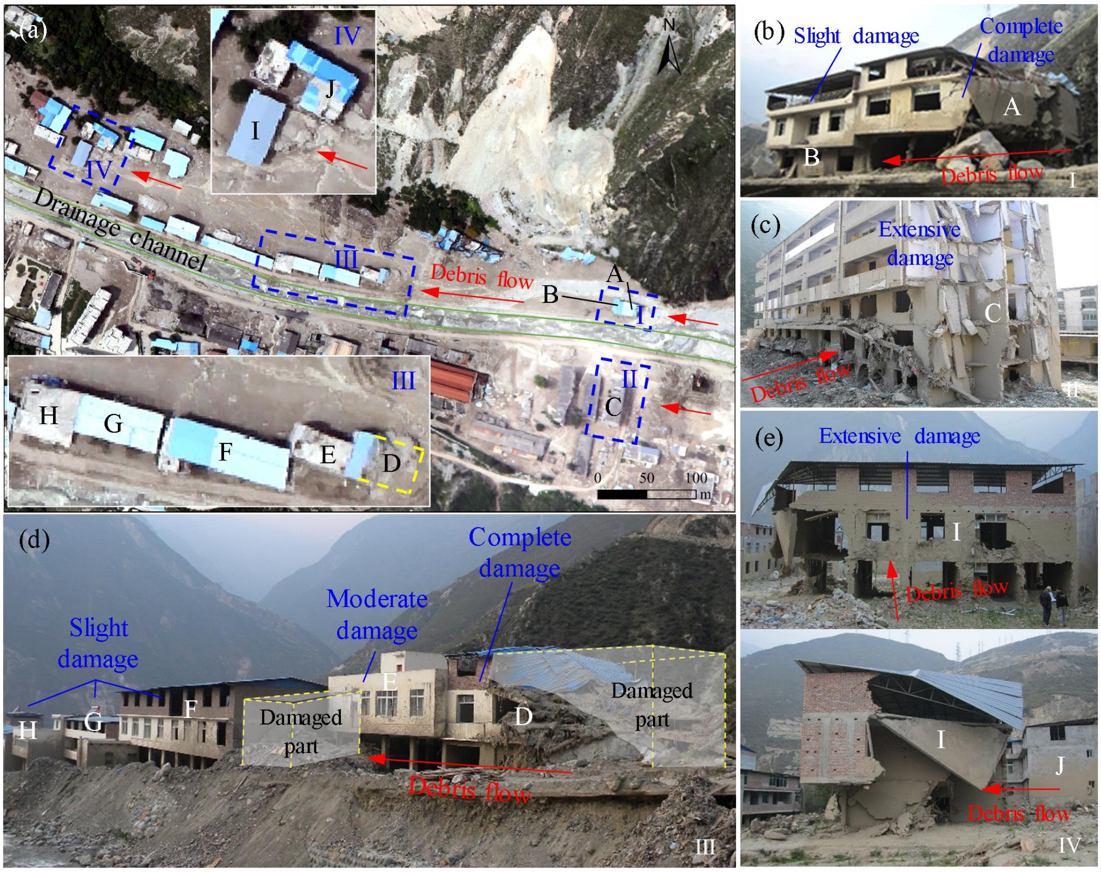

Figure 8. Distribution of damaged-buildings in Qipan gully debris flow event. Orthophoto map is from the Basic Geographic Information Center of Sichuan Province, China, 21 July 2013.

Figure 9. A deflection wall used to protect an entire building ensemble from the impact of medium magnitude events (Galtur Tschafein, Austria) (Holub et al., 2012).

4.3 Effect of the distance to the surrounding buildings

As shown in Fig. 10, the variations in peak impact forces change with the surrounding buildings' distances in conjunction with the influences of azimuth angles. The scenario of the orientation of 90° and opening of 0.4 (***Or***90-***Op***0.4-***A***x-***D***x) is taken as an example, and the background value (***Or***90-***Op***0.4-***A***null-***D***null) is still 3694 kN. According to the results of the sensitivity analysis, the most significant second-order effect comes from the interaction between the azimuth angle and distance, which can be divided into an amplification of the shielding effect or a reduction in the canalization effect, as shown in Fig. 10.

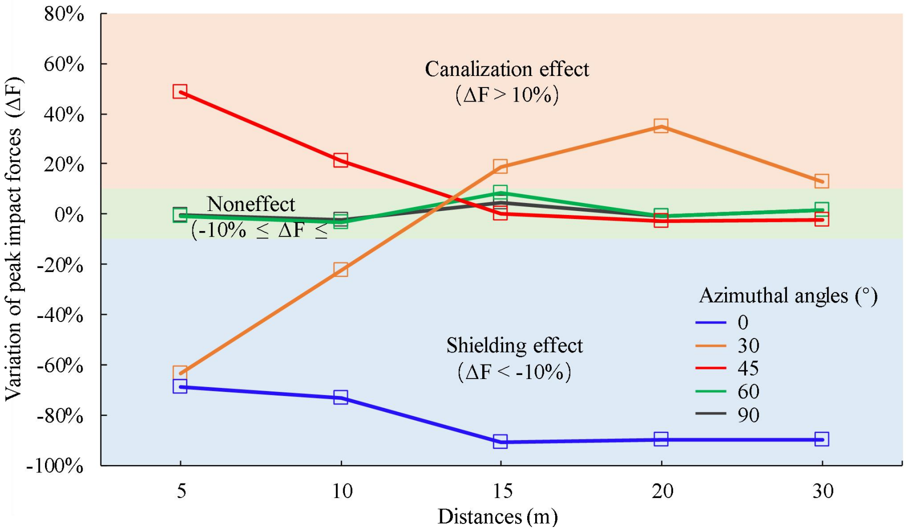

Figure 10. Peak impact forces change with the surroundings' distances under influence of azimuth angles in the scenarios of orientation 90° and opening scale 0.4 (*Or*90-*Op*0.4-*A*x-*D*x).

(1) Amplification of the shielding effect: The peak impact forces are found to be reduced gradually with increasing surrounding building distance in the case of an azimuth angle of 0° (***Or90***-***Op***0.4-***A***0-***D***x), with a 5 m distance yielding 1156 kN and a 30 m distance yielding 372 kN, and the corresponding variations in peak impact forces are approximately -68.71% and -89.93%. The shielding effects at an azimuth angle of 0° are amplified with increasing surrounding distance. This process occurs because there is a broader shielding area further downstream of the surrounding building when the debris flow path is separated by an obstacle at a fixed angle of spread, as shown in Fig. 11. Furthermore, there is likely a small-scale debris flow conflux zone close to the surrounding building, as shown in the red zone of Fig. 11. Buildings upstream, therefore, may suffer from a higher impact load in the same debris flow shielding area. As shown in region III of Fig. 8, the lower a buildings' damage degree, the further away the completely damaged building D is in the back shielding area. Building E, next to building D, is exposed to moderate damage, and other shielding-protected buildings, such as buildings F, G and H, experience only slight damage from lateral abrasion and accumulation. However, the amplified shielding effect inevitably disappears further downstream due to the confluence of debris flow run-off. The range of the shielding area

mainly depends on the debris flow properties, especially the friction coefficient and dynamic viscosity (Liang et al., 2021). Further investigation of the effective shielding-protection area is needed.

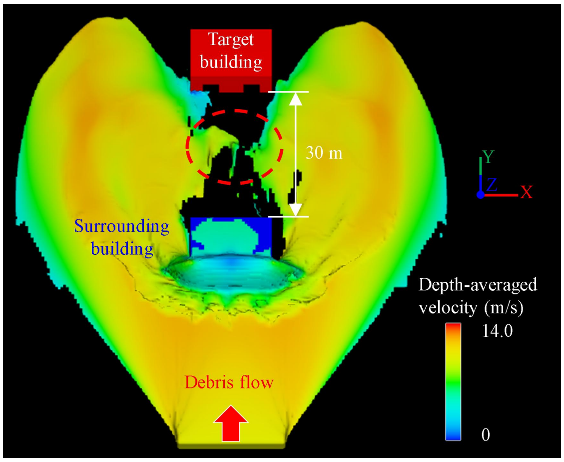

Figure 11. There is the lower debris flow intensities further away surrounding building within a shielding area, in scenario of *Or*90-*Op*0.4-*A*0-*D*30 at simulation time of 8.0 s. The local debris flow conflux is delineated with red dotted line (The snapshot is rotating 30° counterclockwise about the X axis based on plan view, similarly hereinafter).

(2) Reduction in the canalization effect: The canalization effect mainly occurs under a surrounding building azimuth angle of 45°, as mentioned above; however, this kind of effect could be lessened under the influence of the surrounding buildings' distances. As shown by the red line in Fig. 10, the maximum peak impact force under an azimuth angle 45°, with a value of 5482 kN, appears with a distance 5 m (***Or***90-***Op***0.4-***A***45-***D***5). Then, the peak impact forces decrease rapidly with greater distances, especially in the distance range of less than 15 m. The peak impact force at a distance of 15 m (***Or***90-***Op***0.4-***A***45-***D***15) is reduced to 3692 kN, which is very close to the background value (3694 kN). It is indicated that the canalization effect under an azimuth angle of 45° may have vanished completely at this point. As shown in the computational results at 8.0 s in Fig. 12, the increase in flow velocity in the narrowed flow paths due to building blockage decreases with increasing surrounding building distances. The increased-velocity debris flows, on the other hand, tend to flow away from the target building in the cases of greater surrounding building distances. Therefore, the variations in peak impact forces are close to 0 due to the lower flow velocity and fewer intruding materials in the scenarios of surrounding building distances beyond 15 m. In general, a greater distance results in a lower impact force.

A smaller surrounding building distance, however, does not necessarily indicate a larger impact force. With surrounding building distances of 5 m and 10 m, impact force shielding effects occur under the condition of an azimuth angle of 30° (***Or***90-***Op***0.4-***A***30-***D***5 and ***Or***90-***Op***0.4-***A***30-***D***10), as shown in Fig. 13, and the corresponding variations in peak impact loads are -63.40% and -22.58%, respectively. The width of the narrowed flow path, which is determined by the factors of the azimuth angle and surrounding building distance, could account for this fact. The flow paths are so narrow, with widths of 1.6 m and 6.6 m, respectively, like bottlenecks, that not much flow passes through them, as shown in Fig. 13a and Fig. 13b. Thereafter, the canalization effect occurs at distances beyond 15 m and reduces and even disappears gradually with increasing surrounding building distance and the corresponding wider flow paths. It is found that the ratio of the width of the narrowed flow path to the length of the target building has a significant effect on the increase in impact force. The largest 370 peak impact force is most likely to be found under a ratio of approximately one, for example, the ratios of 0.8 in the case of ***Or***90-***Op***0.4-***A***45-***D***5 (Fig. 12a) and 1.1 of ***Or***90-***Op***0.4-***A***30-***D***20 (Fig. 13d).

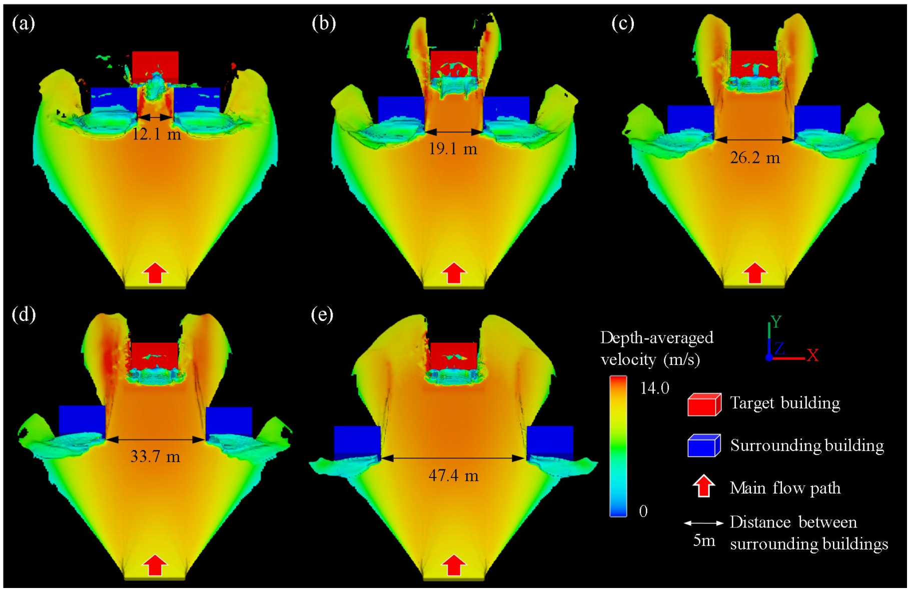

Figure 12. Snapshots for debris flow intensities in scenarios of *Or*90-*Op*0.4-*A*45-*D*x at simulation time of 8.0 s. (a) is case of *Or*90-*Op*0.4-*A*45-*D*5; (b) is case of *Or*90-*Op*0.4-*A*45-*D*10; (c) is case of *Or*90-*Op*0.4-*A*45-*D*15; (d) is case of *Or*90-*Op*0.4-*A*45-*D*20; and (e) is 375 case of *Or*90-*Op*0.4-*A*45-*D*30.

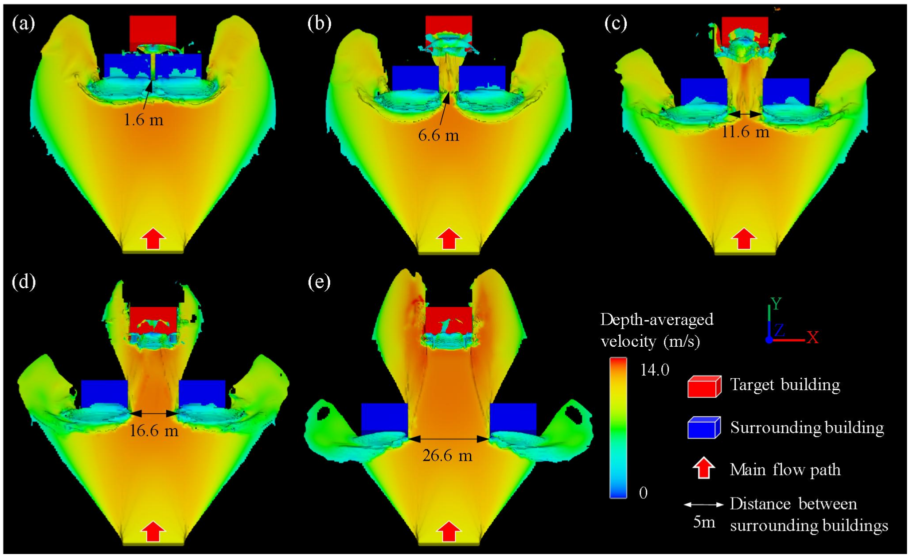

Figure 13. Snapshots for debris flow intensities in the scenarios of *Or*90-*Op*0.4-*A*30-*D*x at simulation time of 8.0 s. (a) is case of *Or*90-*Op*0.4-*A*30-*D*5; (b) is case of *Or*90-*Op*0.4-*A*30-*D*10; (c) is case of *Or*90-*Op*0.4-*A*30-*D*15; (d) is case of *Or*90-*Op*0.4-*A*30-*D*20; and (e) is case of *Or*90-*Op*0.4-*A*30-*D*30.

4.4 Effect of the orientation

4.4.1 Single-factor analysis of orientation

As shown in Fig. 14, the peak impact forces of debris flows are ordered as follows: ***Or***90 > ***Or***60 > ***Or***0 > ***Or***45 ≈ ***Or***30, and the corresponding values are 3563, 2617, 2366, 1982 and 1959 kN, respectively, when only the target building's orientation is considered (***Or***x-***Op***0-***A***null-***D***null). It is generally accepted that the impact load of a debris flow is a comprehensive outcome from many characteristic parameters, including the debris flow density, velocity, impact contact area and approaching angle (Liu et al., 2021). It is assumed that the debris flow density is constant in the computational process of impact forces in the FLOW-3D model.

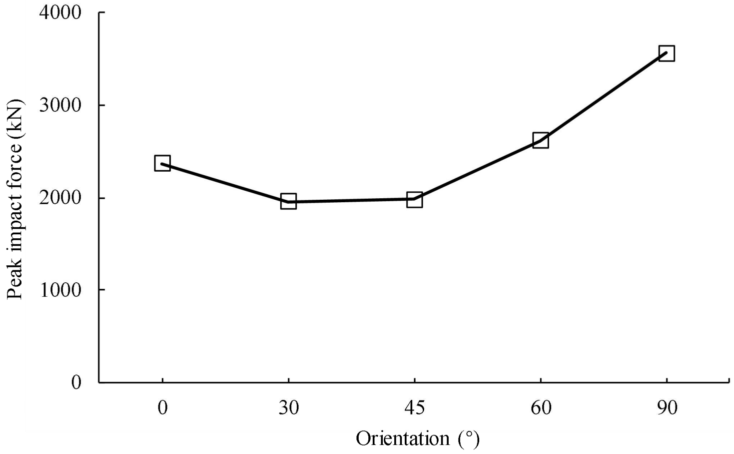

Figure 14. Peak impact forces change with target building's orientations in the scenarios of no openings and no surroundings (*Or*x-*Op*0-*A*null-*D*null).

The impact contact area, a product of the wall length and effective height, where the latter is the minimum value between the wall height and flow depth, can be used to explain the debris flow impact responses in the case of orientations of 0° (***Or***0-***Op***0-***A***null-***D***null) and 90° (***Or***90-***Op***0-***A***null-***D***null). In the simulations shown in Fig. 15a and Fig. 15e, the single wall element, wall B or wall A, is vertically impacted by debris flows, and the surging flows go beyond the wall height. The length of the impacted wall elements, therefore, should contribute to the difference in the peak impact pressures. The mainly impacted wall element in the orientation of 90° - Wall A of 15 m - is obviously longer than that of orientation 0°, wall B of 10 m. A larger contact area results in a greater impact force.

Walls A and B are simultaneously exposed to debris flows and only differ by their orientations 0° and 90°, as shown in Fig. 15b-d. In these cases, the debris flow impact loads, to a large extent, are dominated by the approaching angle, which is defined here as the general, temporally independent angle of the wall element to the main flow path, with a range of 0° (parallel) to 90° (vertical). Generally, there are higher flow velocities and lower surge flow depths in the cases of smaller approaching angles, and vice versa. The highest flow velocity occurs in the neighborhood of wall A, the longest wall of the target building, in the scenario with an orientation 60° (***Or***60-***Op***0-***A***null-***D***null), as shown in Fig. 15d. In contrast, the lowest flow velocity appears near wall A, with an orientation of 30° (***Or***30-***Op***0-***A***null-***D***null), as shown in Fig. 15b. This could be the main reason why the target building with a 60° orientation is under stronger strain than that with a 30° orientation, and that with a 45° orientation is between them. However, even so, better migration performances, such as lower impact loads and larger shielding areas, are produced in these cases than in the case with an orientation of 90°. Similar to this idea, a splitting wedge, with a triangular shape and two downslope-directed sides, was constructed at the process-oriented side of an exposed building to protect against snow avalanches in the Swiss Alps, as shown in Fig. 16. It was confirmed that splitting wedges, with this very distinctive shape, were considerably effective in maintaining its stability and offering a larger protected zone for the other neighboring buildings. It also provides a good model for building protection design in debris flow prone areas. The main criterion for the effective operation of such a structure is avoiding the highest flow velocity - the smallest approaching angle - appearing near the longest wall element.

Last but not least, flip-though impacts, caused by the backwater effect, which is a special phenomenon when debris flow hits a barrier wall, runs up, bounces backward, blocks and converges with the remaining debris (Takahashi, 2007), contribute greatly to the peak impact forces of orientations 0° (***Or***0-***Op***0-***A***null-***D***null) and 90° (***Or***90-***Op***0-***A***null-***D***null), as shown in Fig. 17. The impact forces with an orientation of 0° reach their peak when the debris flow first collides with the wall and runs up. The peak impact load with an orientation of 90° comes from the secondary waves overtaking the flow front, after the flow bounces off the wall, collides and converges with the flow approaching from behind (Iverson et al., 2010; Choi et al., 2018).

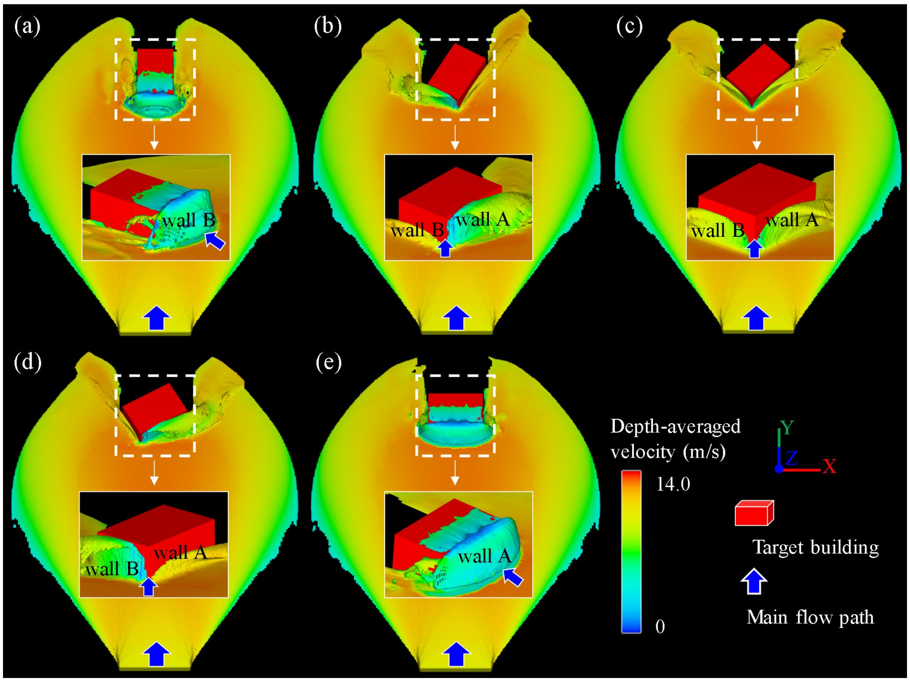

Figure 15. Snapshots for debris flow intensities in scenarios of *Orx*-*Op*0-*A*null-*D*null at simulation time of 8.0 s. (a) is case of *Or*0-*Op*0-*A*null-*D*null; (b) is case of *Or*30-*Op*0-*A*null-*D*null; (c) is case of *Or*45-*Op*0-*A*null-*D*null; (d) is case of *Or*60-*Op*0-*A*null-*D*null; and (e) is case of *Or*90-*Op*0-*A*null-*D*null.

Figure 16. Splitting wedge directly connected to the exposed object (Davos Frauenkirch, Switzerland) (Holub et al., 2012).

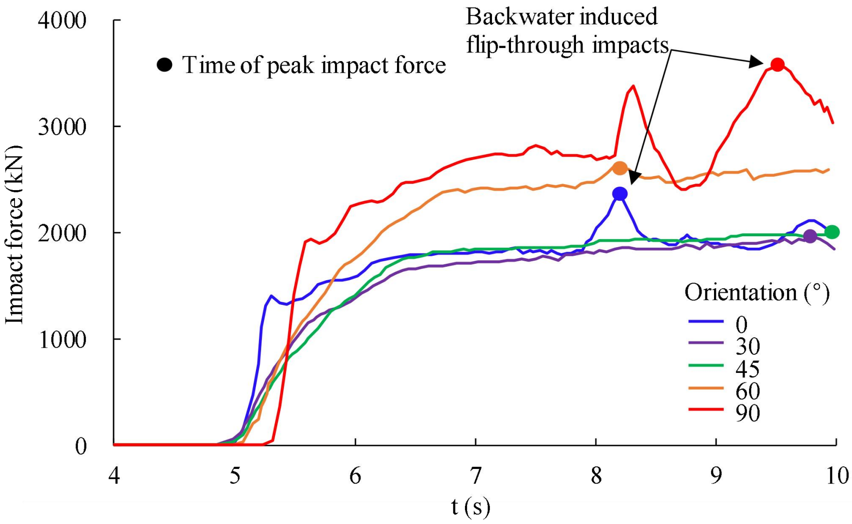

Figure 17. Impact forces time history with changing orientations in the scenarios of *Or*x-*Op*0-*A*null-*D*null after simulation time of 4.0 s. The time of peak impact force are marked with dot.

4.4.2 Interaction between orientation and surroundings

The single-factor analysis of orientation explained why the buildings with orientations of 30°, 45° and 60° have better migration effects. This knowledge has to be reconsidered, however, when the effect overlaps with the surrounding buildings' shielding effects. It is found that buildings with orientations of 30°, 45° and 60° are more likely to be damaged by debris flows within a shielding area. For instance, the maximum peak impact forces with surrounding buildings' distances of 5 m (***Or***60-***Op***0.4-***A***0-***D***5) and 10 m (***Or***60-***Op***0.4-***A***0-***D***10) and an orientation of 60°, as shown in Fig. 18, are different from those of the single-factor analysis of orientation. The protruding parts of the target building caused by the changing orientations and building rotations significantly contribute to the increase in impact forces (Hu et al., 2012; Zeng et al., 2015). A larger protruding portion of a building results in a greater probability of being exposed and corresponding larger impact forces. The largest protruding areas are exposed to debris flows at an orientation of 60°, as shown in Fig. 19d-1 and Fig. 19d-2). This can be confirmed by Fig. 8d. Although the main structure of building E is in the shielding area of building D, its protruding part is still completely destroyed by debris flows.

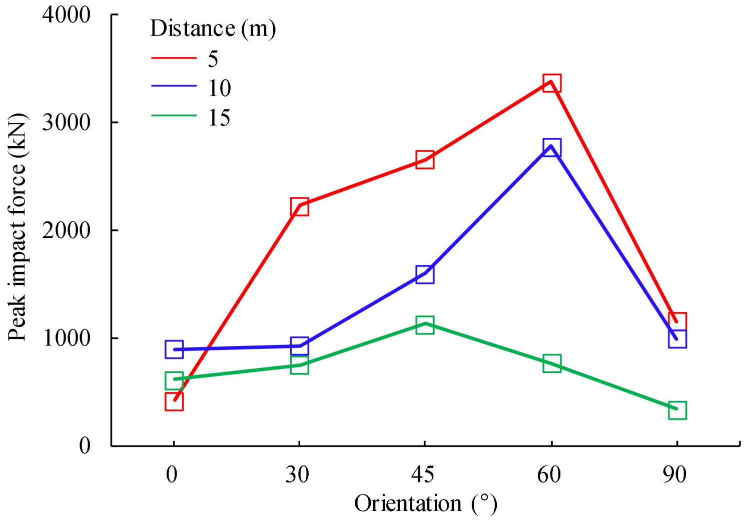

Figure 18. Peak impact forces change with target building's orientations under the shielding effect. Red line shows the case of *Or*x-*Op*0.4-*A*0-*D*5; Blue line shows the case of *Or*x-*Op*0.4-*A*0-*D*10; Red line shows the case of *Or*x-*Op*0.4-*A*0-*D*15.

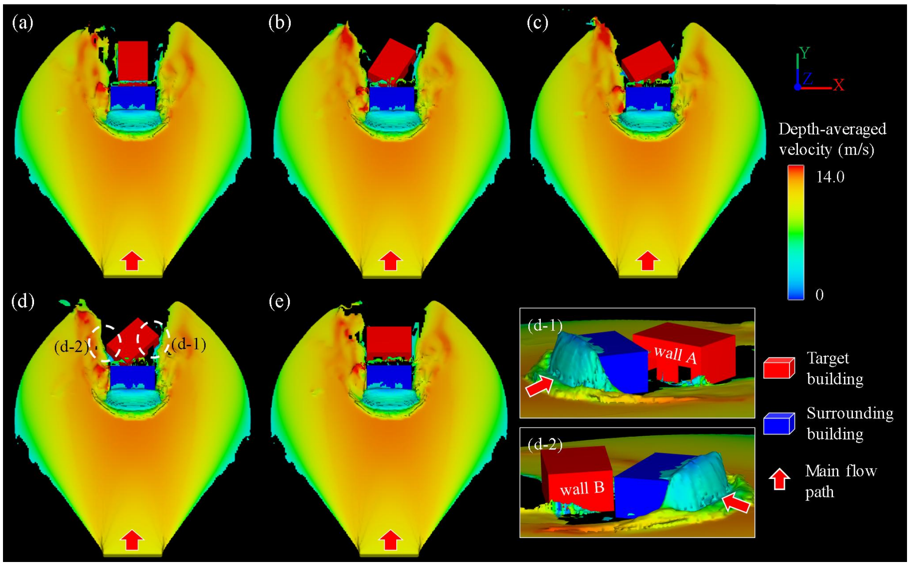

Figure 19. Snapshots for debris flow intensities in scenarios of *Or*x-*Op*0.4-*A*0-*D*5 at simulation time of 8.0 s. (a) is case of *Or*0-*Op*0.4-*A*0-*D*5; (b) is case of *Or*30-*Op*0.4-*A*0-*D*5; (c) is case of *Or*45-*Op*0.4-*A*0-*D*5; (d) is case of *Or*60-*Op*0.4-*A*0-*D*5; (e) is case of *Or*90-*Op*0.4-*A*0-*D*5; (d-1) and (d-2) show that the protruding portions of target building are exposed to debris flow in details.

4.5 Effect of the opening scale

According to the sensitivity analysis results, the opening scale is the least important factor for debris flow impacts, as it yields the minimum first-order effect index, 0.0068, and the minimum total effect index, 0.0255. From the results with an orientation 90° and no surrounding buildings (***Or***90-***Op***x-***A***null-***D***null), shown in Fig. 20, the peak impact forces of the target building change very slightly with increasing opening scale. There is a maximum peak impact force of 3991 kN in the case of openings with a scale of 0.8 (***Or***90-***Op***0.8-***A***null-***D***null), which is approximately 15.8% larger than the 3446 kN of openings with a scale of 0.2 (***Or***90-***Op***0.2-***A***null-***D***null). Interestingly, the impact responses of the target building are different with different opening scales. Specifically, there are smaller impact forces in the cases of larger opening scales when only wall A of the target building is impacted, that is, in the early stage of debris flow impact from 5.2 s to 6.2 s, as shown in Fig. 21. In this stage, the maximum impact pressure of 791 kN of opening scale 0.8 is approximately half of the 1557 kN of opening scale 0.2; this is due to the difference in the effective impacted areas. From this perspective, the mitigation performance of single wall elements with more openings is proven (Mazzorana et al., 2014; Gems et al., 2016). Thereafter, the impact load of the overall building increases rapidly following the abundant intrusion of materials through openings after 6.2 s, as shown in Fig. 21. Due to the greater accessibility and higher flow velocity, there is faster growth in impact pressure in the scenarios with the larger opening scales. Finally, after the two above-described impact stages are combined, there are only slight differences between multiple scales of openings in terms of peak impact forces. This indicates that the mitigation function of openings for the whole building is very limited if the time for materials intrusion is sufficient.

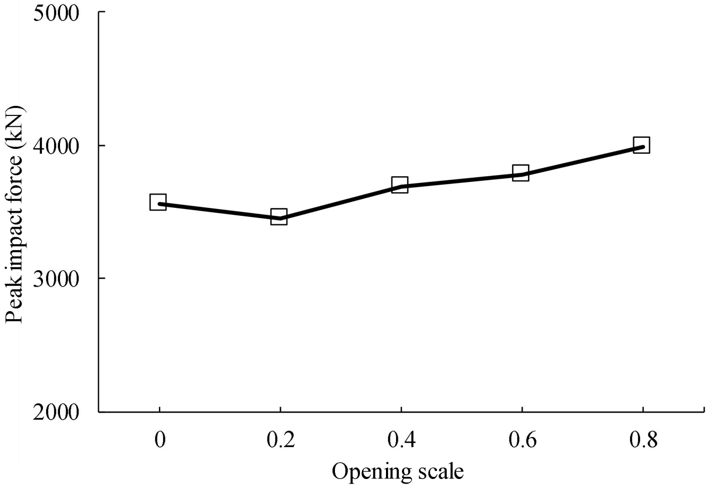

Figure 20. Peak impact forces change with target building's opening scale in the scenarios of *Or*90-*Op*x-*A*null-*D*null.

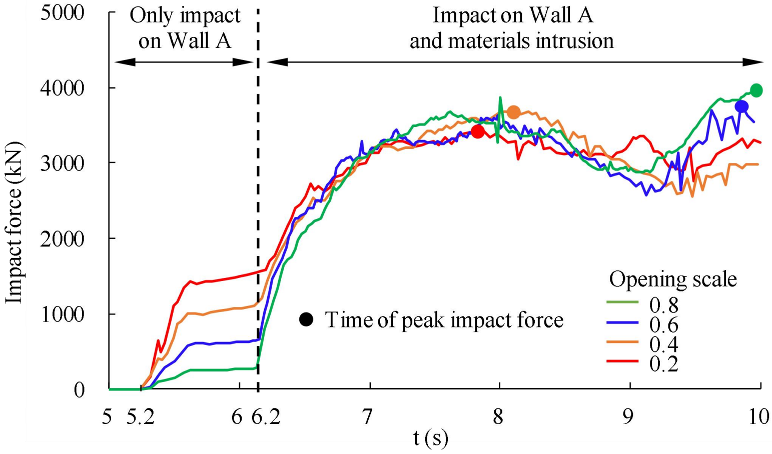

Figure 21. Impact forces time history with changing opening scales in the scenarios of *Or*90-*Op*x-*A*null-*D*null after simulation time of 5.0 s. The time of peak impact force are marked with dot.

5 Conclusions and outlook

The effects of representative built environment parameters on the debris flow impacts on a whole building were explored through FLOW-3D simulations after validation with published experimental results. Four parameters influencing the impact responses of the whole building induced by debris flows were considered in this study: the orientation and opening scale of the target building and the azimuthal angle and distance of the surrounding buildings. The debris flow impact performance was evaluated using the measurable indicator of the peak impact force acting on the overall building. Based on the findings and discussion, the following conclusions can be drawn:

(1) The GSA based on metamodels with 160 cases reveals that the ranking of the importance of the built environment parameters on debris flow impacts from the results of total effect indices is as follows: azimuth angle (***A***) > orientation (***O*r**) > distance (***D***) > opening scale (***Op***). The azimuth angle of the surrounding buildings alone contributes to 51.44% of the overall variance of the debris flow peak impact load. The properties of the surrounding buildings, including the azimuth angle and distance, are found to have a more significant influence on the peak impact forces.

(2) The azimuth angle has a shielding or canalization effect on debris flow impacts. The shielding effect, a form of reducing impact pressures, mainly appears in the scenarios with a surrounding building azimuth angle of 0°. The canalization effect, caused by narrowing and redirecting of the flow path, is a form of increasing impact forces and occurs at an azimuth angle of 45°. A deflection wall for building protection is recommended, as this provides a shielding effect. The interaction between the azimuth angle and distance can be divided into the amplification of the shielding effect and the reduction in the canalization effect. The former is where buildings are less impacted with a limited increase in distance within a shielding area. Further investigation on the effective area of shielding protection is needed. The latter is where the peak impact force induced by the canalization effect decreases rapidly with a greater distance. The ratio of the width of the narrowed flow path

to the length of the target building has a significant effect on the variation in the impact forces, and the maximum peak impact pressure appears at a ratio of approximately one.

(3) These parameters involving the building's impact response, including the impact contact area, approaching angle and flip-though impact, contribute to the debris flow impact forces when only the orientation factor is considered. A splitting wedge is recommended for an effective design mitigating the threat of debris flow, and the main criterion is avoiding the highest flow velocity - the smallest approaching angle - appearing near the longest wall element. The buildings with orientations of 30°, 45° and 60° are more likely to be impacted by debris flows in a shielding area due to the exposed protruding parts produced by the building's rotations. As far as openings are concerned, although the mitigation performance of this single wall element has been proven, a limited effect on the whole building is observed when there is enough time for material intrusion.

Author contribution. XH and ZZ contributed to the original idea and study design. XH, ZZ and GX participated in field survey. XH and ZZ conducted the simulation and analyse. XH wrote the original manuscript, and ZZ and GX provided comments and revised the manuscript. All the co-authors contributed to scientific interpretations of the results.

Competing interests. The authors declare that they have no conflict of interest.

Financial support. This research has been supported by the National Natural Science Foundation of China (grant No. 41907396), the Science and Technology Research Program of Chongqing Municipal Education Commission (grant No. KJQN201900535), the Chongqing Normal University Founding Program (grant No. 21XWB007), the Chongqing Normal University Postgraduate Research and Innovation Project (grant No. YKC21047) and the Scientific Research Project of Department of Natural Resources of Sichuan Province (grant No. KJ-2021-14).

References

Booker, A. J., Dennis, J. E., Rank, P. D., Serafini, D. B., Torczon, V., and Trosset, M. W. A rigorous framework for optimization of expensive functions by surrogates, Structural Optimization, 17, 1-13, https://doi.org/10.1007/BF01197708, 1999.

Chen, M., Tang, C., Zhang, X., Xiong, J., and Li, M.: Quantitative assessment of physical fragility of buildings to the debris flow on 20 August 2019 in the Cutou gully, Wenchuan, southwestern China, Engineering Geology, 293, 106319, https://doi.org/10.1016/j.enggeo.2021.106319, 2021.

Choi, S. K., Lee, J. M., and Kwon, T. H.: Effect of slit-type barrier on characteristics of water-dominant debris flows: small-scale physical modeling, Landslides, 15, 111-122, https://doi.org/10.1007/s10346-017-0853-4, 2018.

Faisal, N. A. A., Ghani, A., and Salim, N.: The ability of wall openings to reduce flood induced forces on residential building, International Journal of GEOMATE, 14, 63-69, https://doi.org/10.21660/2018.46.7306, 2018.

Franco, A., Moernaut, J., Schneider-Muntau, B., Strasser, M., Gems, B.: Triggers and consequences of landslide-induced impulse waves-3D dynamic reconstruction of the Taan Fiord 2015 tsunami event, Engineering Geology, 294, 106384, https://doi.org/10.1016/j.enggeo.2021.106384, 2021.

Fuchs, S., Keiler, M., and Zischg, A. P.: A spatiotemporal multi-hazard exposure assessment based on property data. Nat. Hazards Earth Syst. Sci., 15, 2127-2142, https://doi.org/10.5194/nhess-15-2127-2015, 2015.

Fuchs, S., Keiler, M., Ortlepp, R., Schinke, R., and Papathoma-Köhle, M.: Recent advances in vulnerability assessment for the built environment exposed to torrential hazards: Challenges and the way forward, Journal of Hydrology, 575, 587-595, https://doi.org/10.1016/j.jhydrol.2019.05.067, 2019.

Fuchs, S., Ornetsmüller, C., Totschnig, R.: Spatial scan statistics in vulnerability assessment: an application to mountain hazards, Nat Hazards, 64, 2129-2151, https://doi.org/10.1007/s11069-011-0081-5, 2012.

Fuchs, S., Röthlisberger, V., Thaler, T., Zischg, A., and Keiler, M.: Natural hazard management from a coevolutionary perspective: Exposure and policy response in the European Alps, Annals of the American Association of Geographers, 107, 382-392, https://doi.org/10.1080/24694452.2016.1235494, 2017.

Gao, L., Zhang, L. M., and Chen, H. X.: Two-dimensional simulation of debris flow impact pressures on buildings, Engineering Geology, 226, 236-244, https://doi.org/10.1016/j.enggeo.2017.06.012, 2017.

Gems, B., Mazzorana, B., Hofer, T., Sturm, M., Gabl, R., and Aufleger, M.: 3-D hydrodynamic modelling of flood impacts on a building and indoor flooding processes, Nat. Hazards Earth Syst. Sci., 16, 1351-1368, https://doi.org/10.5194/nhess-16-1351-2016, 2016.

Hirt, C. W., Nichols, B. D.: Volume of fluid (VOF) method for the dynamics of free boundaries, J. Comput. Phys., 39, 201-225, https://doi.org/10.1016/0021-9991(81)90145-5, 1981.

Hirt, C.W., Sicilian, J. M.: A porosity technique for the definition of obstacles in rectangular cell meshes, 4th International Conference on Numerical Ship Hydrodynamics. https://trid.trb.org/view/394627, 1985.

Hoffman, R. M., Sudjianto, A., Du, X., and Stout, J.: Robust piston design and optimization using piston secondary motion analysis (No. 2003-01-0148) (SAE Technical Paper), https://doi.org/10.4271/2003-01-0148, 2003.

Holub, M., and Fuchs, S.: Mitigating mountain hazards in Austria - legislation, risk transfer, and awareness building, Nat. Hazards Earth Syst. Sci., 9, 523-537, https://doi.org/10.5194/nhess-9-523-2009, 2009.

Holub, M., Suda, J., and Fuchs, S.: Mountain hazards: reducing vulnerability by adapted building design, Environ Earth Sci, 66, 1853-1870, https://doi.org/10.1007/s12665-011-1410-4, 2012.

Hu, K. H., Cui, P., and Zhang, J. Q.: Characteristics of damage to buildings by debris flows on 7 august 2010 in zhouqu, western china, Nat. Hazards Earth Syst. Sci., 12, 2209-2217, https://doi.org/10.5194/nhess-12-2209-2012, 2012.

Hu, Y., Chen, M., and Zhou, J.: Numerical simulation of the entrainment effect during mass movement in high-speed debris avalanches, Arabian Journal of Geosciences, 12, 14, https://doi.org/10.1007/s12517-018-4199-6, 2019.

Hu, Y., Yu, Z., and Zhou, J.: Numerical simulation of landslide-generated waves during the 11 October 2018 Baige landslide at the Jinsha River, Landslides, 17, 2317-2328, https://doi.org/10.1007/s10346-020-01382-x, 2020.

Huang, X., and Tang, C.: Formation and activation of catastrophic debris flows in Baishui River basin, Sichuan Province, China, Landslides, 11, 955-967, https://doi.org/10.1007/s10346-014-0465-1, 2014.

Isobe, D., and Tanaka, S.: Sequential simulations of steel frame buildings under multi-phase hazardous loads during earthquake and tsunami, Frontiers in Built Environment, 7, 1-17, https://doi.org/10.3389/fbuil.2021.669601, 2021.

Iverson, R. M., Logan, M., Lahusen, R. G., and Berti, M.: The perfect debris flow? Aggregated results from 28 large-scale experiments, Journal of Geophysical Research Earth Surface, 115, F03005, https://doi.org/10.1029/2009JF001514, 2010.

Jakob, M., Stein, D., and Ulmi M.: Vulnerability of buildings to debris flow impact, Nat Hazards, 60, 241-261, http://doi.org/10.1007/s11069-011-0007-2, 2012.

Jones, W. P., and Launder, B. E.: The prediction of laminarization with a two-equation model of turbulence, Int. J.Heat Mass Tran., 15, 301- 314, https://doi.org/10.116/0017-9310(72)90076-2, 1972.

Kim, M. J., Lee, S. R., Jeon, J. S., and Yoon, S.: Sensitivity analysis of bentonite buffer peak temperature in a high-level waste repository, Annals of Nuclear Energy, 123, 190-199, https://doi.org/10.1016/j.anucene.2018.09.020, 2019.

Kim, M., Lee, S., Kwon, T., Choi, S., and Jeon, J.: Sensitivity analysis of influencing parameters on slit-type barrier performance against debris flow using 3D-based numerical approach, International Journal of Sediment Research, 36, 50-62, https://doi.org/10.1016/j.ijsrc.2020.04.005, 2021.

Kleijnen, J. P. C.: Regression and Kriging metamodels with their experimental designs in simulation: A review[J]. European Journal of Operational Research, 256, 1-16, http://dx.doi.org/10.1016/j.ejor.2016.06.041, 2016.

Kucherenko, S., Albrecht, D., and Saltelli, A.: Exploring multi-dimensional spaces: a Comparison of Latin Hypercube and Quasi Monte Carlo Sampling Techniques. https://doi.org/10.48550/arXiv.1505.02350, 2015.

Liang, H., Li, J., Liu, F., Zhang, L., Gang, F., Li, M., and He, S.: Simulation of debris flow impacting bridge pier tests based on smooth particle hydromechanics method, Rock and soil mechanics, 42, 1473-1484, https://doi.org/10.16285/j.rsm.2020.1107, 2021 (in Chinese with English abstract).

Liu, C., Yu, Z., and Zhao, S.: A coupled SPH-DEM-FEM model for fluid-particle-structure interaction and a case study of Wenjia gully debris flow impact estimation, Landslides, 18, 2403-2425, https://doi.org/10.1007/s10346-021-01640-6, 2021.

Lugni, C., Brocchini, M., and Faltinsen, O. M.: Wave impact loads: the role of the flip-through. Physics of Fluids, 18, 122101, https://doi.org/10.1063/1.2399077, 2006.

Luo, H. Y., Fan, R. L., Wang, H. J., and Zhang, L. M.: Physics of building vulnerability to debris flows, floods and earth flows, Engineering Geology, https://doi.org/10.1016/j.enggeo.2020.105611, 2020.

Manawasekara, C., Mizutani, N., and Aoki, S.: Influence of openings and orientation on tsunami generated forces on buildings, Journal of Disaster Research, 11, 670-679, https://doi.org/10.20965/jdr.2016.p0670, 2016.

Mazzorana, B., Simoni, S., Scherer, C., Gems, B., and Keiler, M.: A physical approach on flood risk vulnerability of buildings, Hydrol. Earth Syst. Sci., 18, 3817-3836, https://doi.org/10.5194/hessd-11-1411-2014, 2014.

Mead, S. R., Magill, C., Lemiale, V., Thouret, J. C., Prakash, M.: Examining the impact of lahars on buildings using numerical modelling, Nat. Hazards Earth Syst. Sci., 17, 703-719, https://doi.org/10.5194/nhess-17-703-2017, 2017.

Méjean, S., Guillard, F., Faug, T., and Einav, I.: Length of standing jumps along granular flows down smooth inclines, Physical Review Fluids, 5, 034303, https://doi.org/10.1103/PhysRevFluids.5.034303, 2020.

Papathoma-Köhle, M., Gems, B., Sturm, M., and Fuchs, S.: Matrices, curves and indicators: A review of approaches to assess physical vulnerability to debris flows, Earth-Science Reviews, 171, 272-288, http://doi.org/10.1016/j.earscirev.2017.06.007, 2017.

Papathoma-Köhle, M., Schlögl, M., and Fuchs, S.: Vulnerability indicators for natural hazards: an innovative selection and weighting approach, Scientific Reports, 9, 15026, https://doi.org/10.1038/s41598-019-50257-2, 2019.

Papathoma-Köhle, M.: Vulnerability curves vs. vulnerability indicators: application of an indicator-based methodology for debris-flow hazards, Nat. Hazards Earth Syst. Sci., 16, 1771-1790, https://doi.org/10.5194/nhess-16-1771-20162016, 2016.

Postacchini, M., Zitti, G., Giordano, E., Clementi, F., and Lenci, S.: Flood impact on masonry buildings: the effect of flow characteristics and incidence angle, Journal of Fluids and Structures, 88, 48-70, https://doi.org/10.1016/j.jfluidstructs.2019.04.004, 2019.

Prieto, J. A., Journeay, M., Acevedo, A. B., Arbelaez, J. D., and Ulmi, M.: Development of structural debris flow fragility curves (debris flow buildings resistance) using momentum flux rate as a hazard parameter. Engineering Geology, 239, 144-157, https://doi.org/10.1016/j.enggeo.2018.03.014, 2018.

Saltelli, A., Annoni, P., Azzini, I., Campolongo, F., and Tarantola, S.: Variance based sensitivity analysis of model output. Design and estimator for the total sensitivity index, Computer Physics Communications,181, 259-270, https://doi.org/10.1016/j.cpc.2009.09.018, 2010.

Sarrazin, F., Pianosi, F., and Wagener, T.: Global sensitivity analysis of environmental models: Convergence and validation, Environmental Modelling and Software, 79, 135-152, https://doi.org/10.1016/j.envsoft.2016.02.005, 2016.

Sobol, I. M., Asotsky, D., Kreinin, A., and Kucherenko, S.: Construction and comparison of high-dimensional Sobol' generators, Wilmott, 2011, 64-79, https://doi.org/10.1002/wilm.10056, 2011.

Sobol, I. M.: Sensitivity estimates for nonlinear mathematical models, Mathematical modelling and computational experiments, 1, 407-414, 1993.

Song, D., Chen, X., Zhou, G. G. D., Lu, X., Cheng, G., Chen, Q.: Impact dynamics of debris flow against rigid obstacle in laboratory experiments, Engineering Geology, 291, 106211, https://doi.org/10.1016/j.enggeo.2021.106211, 2021.

Sturm, M., Gems, B., Keller, F., Mazzorana, B., Fuchs, S., Papathoma-Köhle, M., and Aufleger, M.: Understanding impact dynamics on buildings caused by fluviatile sediment transport, Geomorphology, 321, 45-59, https://doi.org/10.1016/j.geomorph.2018.08.016, 2018a.

Sturm, M., Gems, B., Keller, F., Mazzorana, B., Fuchs, S., Papathoma-Köhle, M., Aufleger, M.: Experimental analyses of impact forces on buildings exposed to fluvial hazards, Journal of Hydrology, 565, 1-13, https://doi.org/10.1016/j.jhydrol.2018.07.070, 2018b.

Takahashi, T.: Debris Flow Mechanics, Prediction and Countermeasures, Taylor & Francis Group, London, UK, 2007.

Tang, C., Rengers, N., Asch, T. V., Yang, Y. H., and Wang, G. F.: Triggering conditions and depositional characteristics of a disastrous debris flow event in Zhouqu city, Gansu Province, northwestern China. Nat. Hazards Earth Syst. Sci., 11, 2903-2912, https://doi.org/10.5194/nhess-11-2903-2011, 2011.

Totschnig, R., Sedlacek, W., Fuchs, S.: A quantitative vulnerability function for fluvial sediment transport, Nat Hazards, 58, 681-703, https://doi.org/10.1007/s11069-010-9623-5, 2011.

Yin, Y. P., Huang, B., Chen, X., Liu, G., and Wang, S.: Numerical analysis on wave generated by the Qianjiangping landslide in Three Gorges Reservoir, China. Landslides, 12, 355-364, https://doi.org/10.1007/s10346-015-0564-7, 2015.

Zeng, C., Cui, P., Su, Z., Lei, Y., and Chen, R.: Failure modes of reinforced concrete columns of buildings under debris flow impact, Landslides, 12, 561-571, https://doi.org/10.1007/s10346-014-0490-0, 2015.

Zhang, J., Termaath, S., and Shields M. D.: Imprecise global sensitivity analysis using bayesian multimodel inference and importance sampling. Mechanical Systems and Signal Processing, 148, 107162, https://doi.org/10.1016/j.ymssp.2020.107162, 2021a.

Zhang, S., Zhang, L., Li, X., and Xu, Q.: Physical vulnerability models for assessing building damage by debris flows, Engineering Geology, 247, 145-158, https://doi.org/10.1016/j.enggeo.2018.10.017, 2018.

Zhang, Y., Chen, J., Tan, C., Bao, Y., Han, X., Yan, J., Mehmood, Q.: A novel approach to simulating debris flow runout via a three-dimensional CFD code: a case study of Xiaojia Gully, Bulletin of Engineering Geology and the Environment, 80, 5293-5313, https://doi.org/10.1007/s10064-021-02270-x, 2021b.

Zhuang, Y., Yin, Y., Xing, A., and Jin, K.: Combined numerical investigation of the Yigong rock slide-debris avalanche and subsequent dam-break flood propagation in Tibet, China, Landslides, 17, 2217-2229, https://doi.org/10.1007/s10346-020-01449-9, 2020.